



**HAL**  
open science

## A proton density bubble in the doubly magic $^{34}\text{Si}$ nucleus

A. Mutschler, A. Lemasson, O. Sorlin, D. Bazin, C. Borcea, R. Borcea, Z. Dombradi, J.P. Ebran, A. Gade, H. Iwasaki, et al.

### ► To cite this version:

A. Mutschler, A. Lemasson, O. Sorlin, D. Bazin, C. Borcea, et al.. A proton density bubble in the doubly magic  $^{34}\text{Si}$  nucleus. *Nature Physics*, 2017, 13 (2), pp.142-146. 10.1038/NPHYS3916 . in2p3-01387617

**HAL Id: in2p3-01387617**

**<https://hal.in2p3.fr/in2p3-01387617>**

Submitted on 11 Jul 2017

**HAL** is a multi-disciplinary open access archive for the deposit and dissemination of scientific research documents, whether they are published or not. The documents may come from teaching and research institutions in France or abroad, or from public or private research centers.

L'archive ouverte pluridisciplinaire **HAL**, est destinée au dépôt et à la diffusion de documents scientifiques de niveau recherche, publiés ou non, émanant des établissements d'enseignement et de recherche français ou étrangers, des laboratoires publics ou privés.

# A proton density bubble in the doubly-magic $^{34}\text{Si}$ nucleus

A. Mutschler,<sup>1,2</sup> A. Lemasson,<sup>2,3</sup> O. Sorlin,<sup>2</sup> D. Bazin,<sup>4</sup> C. Borcea,<sup>5</sup> R. Borcea,<sup>5</sup> Z. Dombrádi,<sup>6</sup> J.-P. Ebran,<sup>7</sup>  
A. Gade,<sup>4</sup> H. Iwasaki,<sup>4</sup> E. Khan,<sup>1</sup> A. Lepailleur,<sup>2</sup> F. Recchia,<sup>3</sup> T. Roger,<sup>2</sup> F. Rotaru,<sup>5</sup> D. Sohler,<sup>6</sup>  
M. Stanoiu,<sup>5</sup> S. R. Stroberg,<sup>4,8</sup> J. A. Tostevin,<sup>9</sup> M. Vandebrouck,<sup>1</sup> D. Weisshaar,<sup>3</sup> and K. Wimmer<sup>3,10,11</sup>

<sup>1</sup>*Institut de Physique Nucléaire, IN2P3-CNRS, F-91406 Orsay Cedex, France*

<sup>2</sup>*Grand Accélérateur National d'Ions Lourds (GANIL),*

*CEA/DSM - CNRS/IN2P3, B. P. 55027, F-14076 Caen Cedex 5, France*

<sup>3</sup>*National Superconducting Cyclotron Laboratory, Michigan State University, East Lansing, Michigan 48824, USA*

<sup>4</sup>*Department of Physics and Astronomy and National Superconducting Cyclotron Laboratory,  
Michigan State University, East Lansing, Michigan, 48824-1321, USA*

<sup>5</sup>*IFIN-HH, P. O. Box MG-6, 76900 Bucharest-Magurele, Romania*

<sup>6</sup>*Institute for Nuclear Research, Hungarian Academy of Sciences, P.O. Box 51, Debrecen, H-4001, Hungary*

<sup>7</sup>*CEA, DAM, DIF, F-91297 Arpajon, France*

<sup>8</sup>*TRIUMF, 4004 Westbrook Mall, Vancouver, British Columbia, V6T 2A3 Canada*

<sup>9</sup>*Department of Physics, University of Surrey, Guildford, Surrey GU2 7XH, United Kingdom*

<sup>10</sup>*Department of Physics, Central Michigan University, Mt. Pleasant, Michigan 48859, USA*

<sup>11</sup>*Department of Physics, The University of Tokyo, Hongo, Bunkyo-ku, Tokyo 113-0033, Japan*

(Dated: July 11, 2017)

PACS numbers: to be defined

Many properties of the atomic nucleus, such as vibrations, rotations and incompressibility can be interpreted as due to a two-component quantum liquid of protons and neutrons. Electron scattering measurements on stable nuclei demonstrate that their central densities are saturated, as for liquid drops. In exotic nuclei near the limits of mass and charge, with large imbalances in their proton and neutron numbers, the possibility of a depleted central density, or a “bubble” structure, was discussed in a recurrent manner since the seventies. Here we report first experimental evidence that points to a depletion of the central density of protons in the short-lived nucleus  $^{34}\text{Si}$ . The proton-to-neutron density asymmetry in  $^{34}\text{Si}$  offers the possibility to place constraints on the density and isospin dependence of the spin-orbit force - on which nuclear models have disagreed for decades- and on its stabilizing effect towards limits of nuclear existence.

Microscopic systems composed of atoms or clusters can exhibit intrinsic structures that are bubble-like, with small or depleted central densities. For example, the fullerene molecules, composed of C atoms, are structures with extreme central depletion [1]. In nuclear physics, depletions also arise in nuclei with well-developed cluster structures when clusters are arranged in a triangle or ring-like structure - such as in the triple- $\alpha$  Hoyle state [2, 3]. Unlike such a non-homogeneous, clustered system, central density depletions or bubble-like structures would be much more surprising in homogeneous systems, such as typical atomic nuclei with properties characteristic of a quantum liquid [4].

This hindrance of bubble formation in atomic nuclei is inherent in the nature of the strong force between nucleons, which is strongly repulsive at short distances (below

0.7 fm), attractive at medium range ( $\approx 1.0$  fm) and vanishes at distances beyond 2 fm. In a classical picture, the medium-ranged attraction of nuclear forces implies that nucleons interact strongly and attractively only with immediate neighbors, leading to a saturation of the nuclear central density,  $\rho_0$ . Quantum mechanically, the delocalization of nucleons [5] leads to a further homogeneity of the density. Extensive precision electron scattering studies from stable nuclei [6] confirm that their central densities are essentially constant, with  $\rho_0 \approx 0.16 \text{ fm}^{-3}$ , independent of the number of nucleons  $A$ . As a consequence, like a liquid drop, the nuclear radii and volumes increase as  $A^{1/3}$  and as  $A$ , respectively. Thus, *a priori*, bubble-like nuclei with depleted central densities are unexpected.

Historically, the possibility of forming bubble nuclei was investigated theoretically in intermediate-mass [7–10], superheavy [11] and hyperheavy systems [12]. In general, central depletions will arise from a reduced occupation of single particle orbits with low angular momentum  $\ell$ . These wave functions extend throughout the nuclear interior whereas those with high- $\ell$  are more excluded by centrifugal forces. For example, in a comparison of the charge densities of  $^{206}\text{Pb}$  and  $^{205}\text{Tl}$ , the contribution from  $\ell=0$  orbits (there  $3s$ ) is peaked at the nuclear center [13]. The amplitude of this central depletion in  $^{205}\text{Tl}$  is of order 11%. A much larger central depletion of protons, of about 40% compared to stable  $^{36}\text{S}$ , was proposed in  $^{34}\text{Si}$  [10, 14] using various mean field approaches, arising from the proton occupancy of the  $2s_{1/2}$  orbital. However, recent theoretical calculations suggest that nuclear correlations act to smoothen these orbital occupancies in both the heavy and superheavy nuclei [15, 16] and in  $^{34}\text{Si}$  [17]. Here, we use the one-proton removal ( $-1p$ ) reaction technique to show that the  $2s_{1/2}$  proton orbit in  $^{34}\text{Si}$  is in fact essentially empty, in contrast to  $^{36}\text{S}$  where

this  $2s_{1/2}$  orbit is almost fully occupied by 1.7(4) protons compared to the maximum occupancy of 2 [18, 19].

A beam of  $4 \times 10^5$   $^{34}\text{Si}$  nuclei per second was produced by the fragmentation of a 140 MeV/u  $^{48}\text{Ca}$  primary beam on a  $846 \text{ mg}\cdot\text{cm}^{-2}$  thick  $^9\text{Be}$  target at the Coupled Cyclotron Facility at the National Superconducting Cyclotron Laboratory. The  $^{34}\text{Si}$  then impinged on a  $^9\text{Be}$  secondary target ( $100 \text{ mg}\cdot\text{cm}^{-2}$ ) producing  $^{33}\text{Al}$  nuclei through the  $(-1p)$  reaction. These  $^{33}\text{Al}$  residues were identified through their measured energy-loss in an ionization chamber located at the focal plane of the S800 spectrograph, and their time-of-flight between two scintillators placed at the object and image focal planes of the device. Their trajectories were obtained from their positions measured at two cathode-readout drift chambers.

Prompt  $\gamma$ -rays, originating from the in-flight decay of excited  $^{33}\text{Al}$  produced during the reaction, were detected in coincidence with the  $^{33}\text{Al}$  residues in the seven modules of the GREINA array [20] that surrounded the target at angles near  $90^\circ$  and  $58^\circ$ . Event-by-event Doppler reconstruction was performed using the deduced  $^{33}\text{Al}$  velocity at the mid-target position, the position reconstruction on the target, and the  $\gamma$ -ray detection angle – determined from the position of the greatest energy deposition in the GREINA array. An absolute in-flight efficiency of 6.5% and an energy resolution of  $\sigma \simeq 2 \text{ keV}$ , respectively, were obtained at 1 MeV, based on the use of calibrated sources and GEANT4 simulations [21] to account for the Lorentz boost. A systematic uncertainty of 0.25% is estimated on the  $\gamma$  energy centroid.

The  $\gamma$  singles (first row of Fig. 1),  $\gamma - \gamma$  coincidences (second to third rows of Fig. 1), and the relative  $\gamma$  intensities were used to establish the level scheme of excited states in  $^{33}\text{Al}$ , shown in the left part of Fig. 2. Energies and branching ratios are given for each populated  $^{33}\text{Al}$  final state. The energy of seven  $\gamma$ -rays match, within uncertainties, those observed in the  $\beta$ -decay of  $^{33}\text{Mg}$  [22]. However, the level scheme proposed in Fig. 2 differs significantly from that of Ref. [22] where, unlike in the present work,  $\gamma - \gamma$  coincidences were rarely exploited.

The orbital angular momenta  $\ell$  of the protons removed from  $^{34}\text{Si}$  are determined by comparing, in the right panel of Fig. 2, the experimental ( $\gamma$ -gated) and theoretical longitudinal momentum distributions ( $p_{||}$ ) of the  $^{33}\text{Al}$ . The latter are described in the Section ‘Methods’. The ground state momentum distribution in Fig. 2 is obtained by subtracting contributions from excited states. The  $p_{||}$  distributions of the 0-, 1621-, and 1651-keV states are characteristic of  $\ell=2$  proton removal. The much narrower  $p_{||}$  of the 210- and 3704-keV states suggest  $\ell=0$  assignments.

Normalized spectroscopic factors,  $C^2 S_{norm}^{exp}$ , and proton occupancies of the orbits are derived from the experimental cross sections, as described in Section ‘Methods’. The summed spectroscopic factors for the first three  $\ell=2$  states is  $5.5 \pm 1.0$ , consistent, within uncertainties, with a full occupancy ( $2J+1=6$ ) of the  $1d_{5/2}$  orbit. The weak

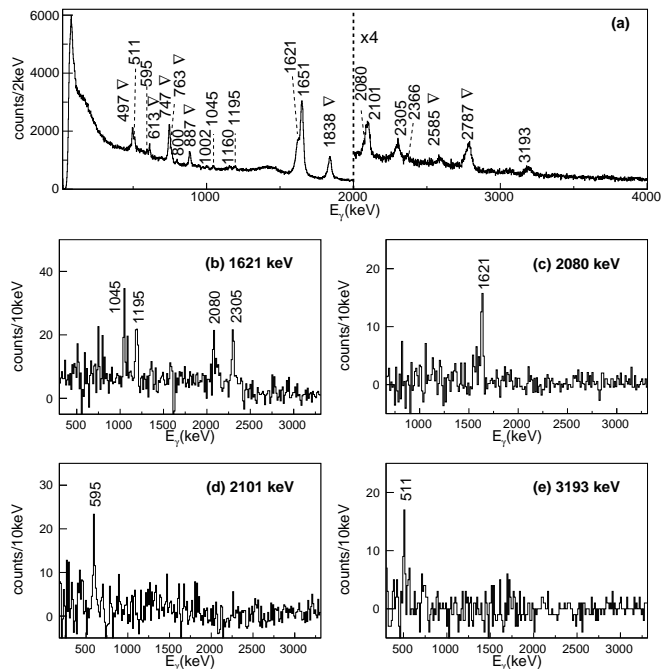


FIG. 1. **Gamma-ray spectra of  $^{33}\text{Al}$ .** Singles (first row) and  $\gamma$ -gated (second to third rows) Doppler-corrected  $\gamma$ -ray spectra of  $^{33}\text{Al}$ . The  $\gamma$ -rays labeled with an empty triangle, accounting for 5.8 % of the cross section, are not produced by the one-proton removal mechanism and are not relevant for determining the proton occupancies. Their origin is discussed in Ref. [19].

population of the 3926 keV state, with a spectroscopic factor of 0.11(3), is tentatively attributed to an  $\ell=2$  proton knockout from the  $1d_{3/2}$  orbit. A proton occupancy of the  $2s_{1/2}$  orbital of 0.17(3) is deduced from the two observed  $\ell=0$  excited states at 2101 and 3704 keV. Assuming, though very unlikely, that the four (unassigned) weakly populated states at 2666, 2696, 2816 and 3193 keV were also  $\ell=0$ , this occupancy would be increased by only 0.07 (3). This very small proton occupancy of the  $2s_{1/2}$  orbital, 10% of that in  $^{36}\text{S}$ , results in a large depletion of the central density of protons in  $^{34}\text{Si}$ .

On the other hand, the *neutron*  $2s_{1/2}$  orbit is essentially fully occupied in  $^{34}\text{Si}$ , with a summed spectroscopic factor value of 2.0(3) being deduced from the corresponding neutron removal reaction from  $^{34}\text{Si}$  [23]. Thus,  $^{34}\text{Si}$  exhibits a large proton-to-neutron density asymmetry that, to our knowledge, has not been revealed in any other nucleus. It is favored because  $^{34}\text{Si}$  can be viewed as a doubly-magic nucleus in which mixing between normally occupied and valence orbits is very limited [23, 24]. The high energy of its first excited state (3.3 MeV), its low reduced transition probability  $B(E2; 0^+ \rightarrow 2^+)$  [25] and the small electric monopole strength  $\rho(E0; 0_1^+ \rightarrow 0_2^+)$  [26] complete this picture of double magicity. Fig. 3 visualizes the changed proton densities and almost unchanged neutron densities between  $^{34}\text{Si}$  and  $^{36}\text{S}$  from Relativistic

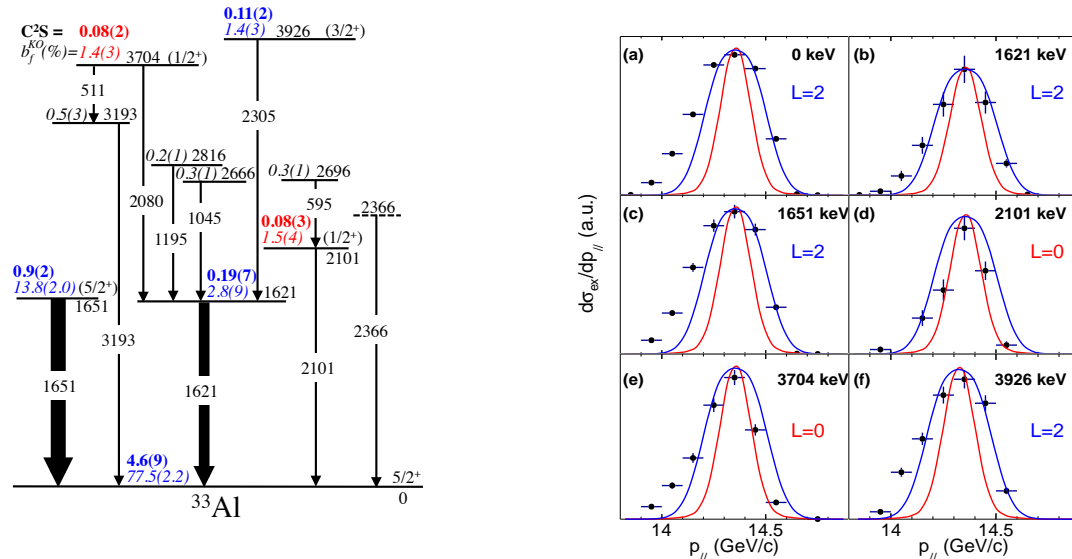


FIG. 2. **Level scheme of  $^{33}\text{Al}$  with parallel momentum distributions of the strongest populated states.** Left: Level scheme of  $^{33}\text{Al}$ , obtained from the  $\gamma$ - $\gamma$  coincidence spectra of Fig. 1, with energies (in keV) and branching ratios  $b_f^{KO}$  (in %). Error bars on the  $b_f^{KO}$  values result from the uncertainty in extracting the intensity of the  $\gamma$  transitions decaying from the corresponding levels. When these levels are fed from higher lying states, the corresponding feeding contribution was subtracted, inducing larger error bars. As fed by many transitions, the branching ratio to the ground state therefore has the largest error bar. The  $J^\pi$  assignments and experimental spectroscopic factors  $C^2 S_{norm}^{exp}$  of the strongest populated states are shown. Uncertainties on the  $C^2 S_{norm}^{exp}$  values are derived from Equation . They include those on  $b_f^{KO}$  discussed above and on the empirical quenching factor  $R_S$ , that amounts to about 20%. Right (a-f): Experimental parallel momentum,  $p_{||}$ , distributions for the strongest populated states in  $^{33}\text{Al}$  (black crosses) are compared to theory, assuming removal of an  $\ell=0$  (red curves) or  $\ell=2$  (blue curves) proton from the  $^{34}\text{Si}$  ground state. As explained in Section 'Methods', the high momentum part of  $p_{||}$  is considered in this comparison. Momentum distributions for weakly populated states ( $b_f^{KO} < 1\%$ ) have insufficient statistics to be exploited. Horizontal bars correspond to the binning on the  $p_{||}$  value. Vertical error bars are deduced from uncertainties on  $b_f^{KO}$  per bin of  $p_{||}$  value.

Hartree-Fock Bogoliubov (RHFB) calculations that use the PKO2 energy density functional [27] and which predict very similar proton and neutron occupancies to those deduced here. It should however be noted that mean field calculations do not all predict similar neutron and proton density profiles in  $^{34}\text{Si}$ . Indeed they are very sensitive to the size of the proton and neutron gaps derived from the choice of functionals, as well as to the treatment of pairing and quadrupole correlations that act to reduce the central density depletion, as found in Ref. [17]. Indeed, this model-dependence of the predictions of the existence of a central depletion was a major motivation to perform the present experiment.

With this differential two-fluid behavior,  $^{34}\text{Si}$  offers unique possibilities to test the density and proton-to-neutron (isospin) dependence of the nuclear spin orbit (SO) potential – which generates most of the shell gaps that stabilize magic nuclei in the chart of nuclides [28, 29]. In most theoretical models, the SO potential can be expressed in terms of the derivative of the proton and neutron densities, with coefficients that differ by a factor of as much as two between various relativistic or non-relativistic approaches (see e.g. the discussions in [11, 29, 31–34]). These as yet unknown density and

isospin dependences of the SO interaction strongly impact (i) the evolution of the spin-orbit interaction and magic numbers as one approaches the drip lines [31, 33], where the surface diffuseness is increased and consequently the SO interaction is expected to be reduced. This influences the binding energies, the lifetimes, and nuclear capture rates of the nuclei close to the neutron drip line that are involved in the synthesis of elements in the Universe beyond Fe through the rapid neutron capture process. This also impacts (ii) the location of a possible island of stability for superheavy nuclei [11] that differ strongly depending on the theoretical models used, and (iii) the puzzling discontinuity in the isotope shifts observed for the Pb isotopes [30, 32], a phenomenon that seems to be accounted for only by a certain category of models. These aspects of the SO force have not previously been accessible to experimental scrutiny as, in the vast majority of nuclei, the saturation of the nuclear forces implies (a) a near-constant central density for protons and neutrons, and (b) an almost universal surface diffuseness. The result is a SO force peaked at the proton and neutron surfaces having a similar strength for all models. The central proton density depletion in  $^{34}\text{Si}$  drives an additional (interior) component of the SO force,

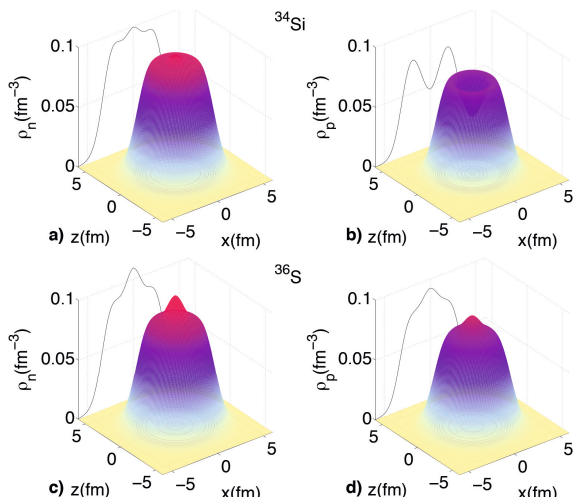


FIG. 3. **Neutron and proton density distributions of the  $^{34}\text{Si}$  and  $^{36}\text{S}$  nuclei.** Neutron (a) and proton (b) density distributions of  $^{34}\text{Si}$  computed using RHF calculations with the PKO2 interaction. (c) and (d) are those for  $^{36}\text{S}$ . While the proton and neutron density distributions are similar in  $^{36}\text{S}$ , they are significantly different in  $^{34}\text{Si}$ , with a sizeable central depletion of protons. Orbital occupancies obtained from these calculations are very similar to those deduced experimentally, providing a visualization of the proton and neutron density distributions in the two nuclei.

with a sign opposite to that at the surface. Therefore, low- $\ell$  nucleons, that can probe the interior of the bubble, should encounter a much weaker overall SO force (e.g. [11, 35]) and display a significantly reduced SO splitting. This prediction is in line with the observed reduction of the neutron  $2p_{3/2} - 2p_{1/2}$  splitting in  $^{35}\text{Si}$  [24], when compared to neighbouring  $N = 21$  isotones. Such a sudden change by a factor of *two* in amplitude is unique on the chart of nuclides and seems clearly connected to the change in central nuclear density observed here. Moreover, having different proton and neutron central densities,  $^{34}\text{Si}$  can be used to constrain the isospin dependence of the SO interaction in an unprecedented manner, for example, by identifying models that predict the correct amplitude of the SO reduction.

Finally, atomic nuclei are usually highly incompressible, the corresponding monopole modes involving very high excitation energies [36, 37]. Exhibiting a central density that is significantly lower than the saturation density,  $^{34}\text{Si}$  may present new (soft) compression modes at low energy with the potential to shed light on the recently observed fragmentation of the giant monopole at low energy in the neutron-rich  $^{68}\text{Ni}$  nucleus [38]. This information would in turn be useful for testing different models of the nuclear equation of state at a density below the saturation density, important for instance in the modeling of the neutron star crust.

## METHODS

The eikonal model and choice of parameters used to calculate the proton removal single-particle cross sections,  $\sigma_{\alpha}^{sp}$ , and the parallel momentum,  $p_{\parallel}$ , distributions of the residues are detailed in Ref. [39]. The shapes of the high momentum parts of these distributions are used in the comparisons with experiment in Fig. 2 as more dissipative collisions, treated only approximately in the eikonal model, affect measured distributions at the lower momenta [40]. In comparing to experiment, the theoretical  $p_{\parallel}$  distributions are convoluted with (i) the momentum dispersion of the secondary beam, (ii) the beam straggling in the target, and (iii) the momentum broadening due the reaction's position within in the target.

The experimental partial cross sections,  $b_f^{KO} \sigma_{inc,KO}^{exp}$ , correspond to the removal of a proton with quantum numbers  $n\ell_J$  from the ground state of  $^{34}\text{Si}$ . Here  $\sigma_{inc,KO}^{exp}$  is the experimental inclusive removal cross section, that amounts to 27.7(1.0) mb, and  $b_f^{KO}$  is the experimental branching ratio (in %) for populating final state  $f$ . Following Ref. [19], the normalized knockout spectroscopic factors are expressed as:

$$C^2 S_{norm}^{exp} = \frac{b_f^{KO} \sigma_{inc,KO}^{exp}}{R_s \sigma_f^{sp}}, \quad (1)$$

where  $\sigma_f^{sp}$  is the theoretical single-particle knockout cross section [39].  $R_s$  accounts for the systematic quenching of measured nucleon knockout cross sections when compared to those calculated when combining these eikonal model  $\sigma_f^{sp}$  with shell model spectroscopy and  $C^2 S$  [41]. With this normalization, the  $C^2 S_{norm}^{exp}$  sum rule (or orbit occupancies) to states in  $^{33}\text{Al}$  are normalized to the maximal occupancy of a given sub-shell, that is  $2J + 1$ .

We are aware that short-range correlations [42] and coupling to collective degrees of freedom [43] usually complicate the determination of spectroscopic factors (or their related shell occupancies and vacancies), which are not directly observable [44–46]. Moreover, present reaction models use effective potentials that do not capture the full microscopic complexity of the nucleus and often induce uncertainties in the deduced results. However, under the reasonable assumption that these effects are similar between neighboring nuclei, here between the closed-shell nuclei  $^{36}\text{S}$  and  $^{34}\text{Si}$ , the consideration of a differential evolution of spectroscopic strengths and occupancies is sensible, a view supported by tests of sum rules for occupancy and vacancy of orbitals derived from experimental cross sections [47]. Error bars on the occupancy values quoted in the main document include statistical and systematical errors, the latter being derived from Ref. [41].

We note that the measured inclusive cross section for the removal of an  $\ell = 0$  proton is about 12 times larger in  $^{36}\text{S}$  than in  $^{34}\text{Si}$ . This directly measured cross-section ratio, attributed to the almost complete depletion of the  $2s_{1/2}$  proton orbit between the two nuclei, has a value that is very similar to the ratio of occupancies derived from the reaction model calculations presented.

It is hoped that the present study will stimulate new developments in the modeling of nuclear reactions and their application to nuclear spectroscopy and further motivate the construction of a high-luminosity electron - radioactive nuclei collider facility that would enable a more direct experimental determination of the proton density distribution in  $^{34}\text{Si}$ .

**Data availability:** Raw data were obtained at the Coupled Cyclotron Facility at the National Superconducting Cyclotron Labo-

ratory, Michigan State University, USA. All other derived data used to support the findings of this study are available from the authors upon request and a thorough explanation of the analysis method can be found in Ref.[48].

**Acknowledgments** This work is supported by the National Science Foundation (NSF) under Grant Nos. PHY-1102511 and PHY-1306297, the OTKA Contract No. K100835, as well as by the Institut Universitaire de France. GRETINA was funded by the US DOE - Office of Science. Operation of the array at NSCL is supported by NSF under Cooperative Agreement PHY-1102511 (NSCL) and DOE under grant DE-AC02-05CH11231 (LBNL). J.A.T acknowledges support of the Science and Technology Facility Council (UK) grant ST/L005743.

**Author Contributions** A.M performed the off-line data analysis, A.Lem, D.W, K.W performed on-line data analysis and checked the integrity of data taking. K.W, A. Lem performed GEANT4 simulations and wrote parts of the offline sorting code. A.G and J.T performed reaction theory calculations. D.B operated the S800 spectrometer. D.W and F.R were responsible for the setting up, calibration and operation of the Gretina array. H.I,K.W helped to setup the Gretina array. The manuscript was prepared by O.S, A.M, J.T, A.G, A.Lem and E.K. J-P.E performed relativistic mean field calculations. Z.D and D.S contributed to the off-line data analysis of the  $\gamma$ -ray spectra and C.B, R.B, E.K, A.Lem, A.Lep, H.I, T.R, M.S, M.V, R.S checked data accumulation on-line. O.S. proposed the experiment and supervised the analysis.

**Author Information** The authors declare no competing financial interests. Readers are welcome to comment the online version of the paper. Correspondence and requests for material should be addressed to O.S. (sorlin@ganil.fr).

- 
- [1] H. P. Schultz, Topological Organic Chemistry. Polyhedranes and Prismanes, *J. Org. Chem.* **30**, 1361-1364 (1965).
- [2] F. Hoyle, On Nuclear Reactions Occurring in Very Hot Stars. I. the Synthesis of Elements from Carbon to Nickel. *Astrophys. J. Suppl. Ser.* **1**, 121 (1954)
- [3] M. Freer and H.O.U. Fynbo, The Hoyle state in  $^{12}\text{C}$ , *Prog. Part. Nucl. Phys.* **78**, 1-23 (2014).
- [4] J.-P. Ebran, E. Khan, T. Nikšić and D. Vretenar, How atomic nuclei cluster?, *Nature* **487**, 341-344 (2012).
- [5] B. Mottelson, Nuclear Structure, Trends in Nuclear Physics, 100 years later, Les Houches, Session LXVI, Amsterdam: Elsevier, 25 (1996).
- [6] R. Hofstadter, Electron Scattering and Nuclear Structure, *Rev. Mod. Phys.* **28**, 214 (1956).
- [7] X. Campi and D. W. L. Sprung, Possible bubble nuclei  $^{36}\text{Ar}$  and  $^{200}\text{Hg}$ , *Phys. Rev. Lett.* **46**, 291-295 (1973).
- [8] K. T. R. Davis, S. J. Krieger and C. Y. Wong, Generalized shells in nuclei: Hartree-Fock calculations for bubble nuclei, *Nucl. Phys. A* **216**, 250-270 (1973).
- [9] E. Khan, M. Grasso, J. Margueron and N. Van Giai, Detecting bubbles in exotic nuclei, *Nucl. Phys. A* **800**, 37-46 (2008).
- [10] M. Grasso *et al.*, Nuclear 'bubble' structure in  $^{34}\text{Si}$ , *Phys. Rev. C* **79**, 034318 (2009).
- [11] M. Bender *et al.*, Shell structure of superheavy nuclei in self-consistent mean-field models, *Phys. Rev. C* **60**, 034304 (1999).
- [12] J. Dechargé, J.-F. Berger, M. Girod, and K. Dietrich, Bubbles and semi-bubbles as a new kind of superheavy nuclei, *Nucl. Phys. A* **716** 55-86 (2003).
- [13] J. M. Cavedon *et al.*, Is the Shell-Model Concept Relevant for the Nuclear Interior?, *Phys. Rev. Lett.* **49**, 978 (1982).
- [14] J.J. Li, W. H. Long, J. L. Song and Q. Zhao, Pseudospin-orbit splitting and its consequences for the central depression in nuclear density, *Phys. Rev. C* **93**, 054312 (2016).
- [15] Y. Z. Wang, Z. Y. Hou, Q. L. Zhang, R. L. Tian, and J. Z. Gu, Pseudospin-orbit splitting and its consequences for the central depression in nuclear density *Phys. Rev. C* **91**, 017302 (2015).
- [16] A. V. Afanasjev and S. Frauendorf, Central depression in nuclear density and its consequences for the shell structure of superheavy nuclei, *Phys. Rev. C* **71**, 024308 (2005).
- [17] J.-M. Yao *et al.*, Beyond-mean-field study of the possible 'bubble' structure of  $^{34}\text{Si}$ , *Phys. Rev. C* **86**, 014310 (2012).
- [18] S. Khan *et al.*, The mass of  $^{35}\text{P}$  and spin-parity assignments for excited  $^{35}\text{P}$  states, *Phys. Lett. B* **156**, 155-158 (1985).
- [19] A. Mutschler *et al.*, Spectroscopy of  $^{35}\text{P}$  using the one-proton knockout reaction, *Phys. Rev. C* **93**, 034333 (2016).
- [20] S. Paschalis *et al.*, The performance of the Gamma-Ray Energy Tracking In-beam Nuclear Array GRETINA, *Nucl. Instr. and Meth. A* **709**, 44-55 (2013).
- [21] S. Agostinelli *et al.*, Geant4: a simulation toolkit, *Nucl. Instr. and Meth. A* **506**, 250-303 (2003).
- [22] V. Tripathi *et al.*, Intruder Configurations in the A=33 Isobars:  $^{33}\text{Mg}$  and  $^{33}\text{Al}$ , *Phys. Rev. Lett.* **101**, 142504 (2008).
- [23] J. Enders *et al.*, Single-neutron knockout from  $^{34,35}\text{Si}$  and  $^{37}\text{S}$ , *Phys. Rev. C* **65**, 034318 (2002).
- [24] G. Burgunder *et al.*, Experimental Study of the Two-Body Spin-Orbit Force in Nuclei, *Phys. Rev. Lett.* **112**, 042502 (2014).
- [25] R.W. Ibbotson *et al.*, Quadrupole Collectivity in  $^{32,34,36,38}\text{Si}$  and the N=20 Shell Closure, *Phys. Rev. Lett.* **80**, 2081 (1998).
- [26] F. Rotaru *et al.*, Unveiling the Intruder Deformed  $0_2^+$  State in  $^{34}\text{Si}$ , *Phys. Rev. Lett.* **109**, 092503 (2012).
- [27] J.-P. Ebran *et al.*, *Phys. Rev. C* **83**, Relativistic Hartree-Fock-Bogoliubov model for deformed nuclei, 064323 (2011).
- [28] O. Sorlin and M. G. Porquet, Evolution of the N=28 shell closure: a test bench for nuclear forces, *Physica Scripta T* **152**, 014003 (2013),
- [29] O. Sorlin and M. G. Porquet, Nuclear magic numbers: New features far from stability, *Prog. Part. Nucl. Phys.* **61**, 602-673 (2008).
- [30] P. -G. Reinhard and H. Flocard, Nuclear effective forces and isotope shifts, *Nucl. Phys. A* **584**, 467-488 (1995).
- [31] M. M. Sharma, G. A. Lalazissis, W. Hillebrandt, and P. Ring, Shell effects in nuclei near the neutron-drip line, *Phys. Rev. Lett.* **72**, 1431 (1994).
- [32] M. M. Sharma, G. Lalazissis, König, and P. Ring, Isospin Dependence of the Spin-Orbit Force and Effective Nuclear Potentials, *Phys. Rev. Lett.* **74**, 3744 (1995).
- [33] G. A. Lalazissis *et al.*, Reduction of the spin-orbit potential in light drip-line nuclei, *Phys. Lett. B* **418**, 7-12 (1998).

- [34] J. W. Holt, N. Kaiser and W. Weise, Nuclear energy density functional from chiral two-nucleon and three-nucleon interactions, *Eur. Phys. J. A* **47**, 128 (2011).
- [35] B. G. Todd-Rutel, J. Pieckarewicz and P.D. Cottle, Spin-orbit splitting in low- $j$  neutron orbits and proton densities in the nuclear interior, *Phys. Rev. C* **69**, 021301 (2004).
- [36] M. N. Harakeh *et al.*, Direct Evidence for a New Giant Resonance at  $80A^{-1/3}$  MeV in the Lead Region, *Phys. Rev. Lett.* **38**, 676 (1977).
- [37] D. H. Youngblood *et al.*, Isoscalar Breathing-Mode State in  $^{144}\text{Sm}$  and  $^{208}\text{Pb}$ , *Phys. Rev. Lett.* **39**, 1188 (1977).
- [38] M. Vandebrouck *et al.*, Measurement of the Isoscalar Monopole Response in the Neutron-Rich Nucleus  $^{68}\text{Ni}$ , *Phys. Rev. Lett.* **113**, 032504 (2014).
- [39] A. Gade *et al.*, Reduction of spectroscopic strength: Weakly-bound and strongly-bound single-particle states studied using one-nucleon knockout reactions, *Phys. Rev. C* **77**, 044306 (2008).
- [40] S. R. Stroberg *et al.*, Single-particle structure of silicon isotopes approaching  $^{42}\text{Si}$ , *Phys. Rev. C* **90**, 034301 (2014).
- [41] J.A. Tostevin and A. Gade, Systematics of intermediate-energy single-nucleon removal cross sections, *Phys. Rev. C* **90**, 057602 (2014).
- [42] V. R. Pandharipande *et al.*, Independent particle motion and correlations in fermion systems, *Rev. Mod. Phys.* **69**, 981 (1997).
- [43] C. Barbieri, Role of Long-Range Correlations in the Quenching of Spectroscopic Factors, *Phys. Rev. Lett.* **103**, 202502 (2009).
- [44] W. H. Dickhoff and C. Barbieri, Self-consistent Green's function method for nuclei and nuclear matter, *Prog. Part. Nucl. Phys.* **52**, 377-496 (2004).
- [45] Th. Duguet, H. Hergert, J. D. Holt and V. Somá, Nonobservable nature of the nuclear shell structure: Meaning, illustrations, and consequences, *Phys. Rev. C* **92**, 034313 (2015).
- [46] R. J. Furnstahl and H.-W. Hammer, Are occupation numbers observable?, *Phys. Lett. B* **531**, 203-208 (2002).
- [47] J. P. Schiffer *et al.*, Test of Sum Rules in Nucleon Transfer Reactions, *Phys. Rev. Lett.* **108**, 022501 (2012).
- [48] A. Mutschler, PhD thesis, Université Paris XI, (2015) Le noyau-bulle de  $^{34}\text{Si}$  : Un outil expérimental pour étudier l'interaction spin-orbite ?, <https://tel.archives-ouvertes.fr/tel-01206188v1>.